17. J. H. Freeman, W. Temple, G. A. Gard, *Vacuum* **34**, 305 (1984).
18. R. S. Nelson, J. A. Hudson, D. J. Mazey, R. C. Piller, *Proc. R. Soc. London Ser. A* **386**, 211 (1983).
19. T. E. Derry and J. P. F. Sellschop, *Nucl. Inst. Methods* **191**, 623 (1981).
20. Y. Lifshitz, S. R. Kasi, J. W. Rabalais, *Phys. Rev. Lett.*, in press.
21. K. Miyake and T. Tokuyama, *Thin Solid Films* **92**, 123 (1982).
22. P. C. Zalm and L. J. Beckers, *Appl. Phys. Lett.* **41**, 167 (1982).
23. J. E. Greene *et al.*, *J. Crystal Growth* **79**, 19 (1986).
24. Y. Morishita, S. Maruno, T. Isu, Y. Nomura, H. Ogala, *ibid.* **88**, 215 (1988).
25. S. M. Rossnagel and J. J. Cuomo, *Vacuum* **38**, 73 (1988).
26. This material is based on work supported by the National Science Foundation on grant DMR-8610597, the Department of Energy on grant DE-FG06-87ER45325, and the state of Texas under the (1988–1989) Advanced Research Program. The authors acknowledge the cooperation of Ch. Gilath and M. Kanter from Soreq Nuclear Research Center, Israel.
2 November 1988; accepted 30 December 1988

Atomic Resolution Imaging of Adsorbates on Metal Surfaces in Air: Iodine Adsorption on Pt(111)

BRUCE C. SCHARDT,* SHUEH-LIN YAU, FRANK RINALDI

The adsorption of iodine on platinum single crystals was studied with the scanning tunneling microscope (STM) to define the limits of resolution that can be obtained while imaging in air and to set a target resolution for STM imaging of metal surfaces immersed in an electrochemical cell. Two iodine adlattice unit cells of slightly different iodine packing density were clearly imaged: $(\sqrt{7} \times \sqrt{7})$ *R*19.1°–I, surface coverage θ_I = 3/7; and (3 × 3)–I, θ_I = 4/9. The three iodine atoms in the $(\sqrt{7} \times \sqrt{7})$ unit cell form a regular hexagonal lattice interatomic distance d_I = 0.424 nanometer, with two atoms adsorbed in threefold hollow sites and one atom adsorbed at an atop site. The (3 × 3) unit cell showed two different packing arrangements of the four iodine atoms exit. In one of the (3 × 3) structures, the iodine atoms pack to form a hexagonal lattice, d_I = 0.417 nanometer, with three of the iodine atoms at twofold adsorption sites and one atom at an atop site. Another packing arrangement of iodine into the (3 × 3) unit cell was imaged in which the iodine atoms are not arranged symmetrically.

THE STM HAS PROVEN A VALUABLE tool under ultrahigh vacuum (UHV) conditions for the atomic resolution imaging of semiconductor, layered semimetal, and metal surfaces (*1, 2*). The application of the STM as an in situ probe of surface structure in heterogeneous catalytic and electrochemical systems requires that the technique be capable of imaging atomic and molecular adsorbates on metal surfaces at atmospheric pressure or in solution or both. Detailed information about adsorbate-substrate bonding, interadsorbate interactions, surface defects, surface diffusion, surface chemical reactions, and interfacial electron-transfer probabilities are some of the potential benefits of STM imaging.

The advantages of the UHV environment for atomic-scale imaging include the ability to prepare well-defined metal surfaces by a variety of means (*3*) and to prepare single atom probe tips by field emission (*4, 5*); however, even with these advantages, there have been only a few examples of atomic-scale imaging of adsorbate-covered metal surfaces in UHV (*6, 7*). The recent imaging of a carbon monoxide–benzene mixed adlattice on a Rh(111) surface in UHV has regenerated hope that the STM can be used to study atomic and molecular adsorbates (*7*).

In contrast to the UHV environment, the majority of atomic resolution studies in the air and liquid environments of importance to catalysis and electrochemistry have been limited to the layered semimetals such as graphite (*2, 8–10*), which can be cleaved in air to form flat, ordered, well-defined surfaces. The only exceptions to this rule are reports describing the imaging in air of a hexagonal Au lattice on Au-coated mica substrate (*11*) and barrier height images of sulfur on Mo (*12*). The imaged Au surface was shown to have a substantial uncharacterized carbon contamination. Barrier height images of sulfur on Mo(001) showed a characteristic p(1 × 2) structure; however, the quality of the images was poor, preventing assignment of the sulfur adsorption sites. Solution studies of metal surfaces have been limited to examination of terrace structures (*13, 14*).

In order to probe the limits of resolution that the STM can be expected to yield in air and ultimately in solution, we have examined iodine-dosed Pt single crystals. The choice of iodine adsorption on Pt as an initial system to study originates in its historical importance to the electrochemistry of well-defined surfaces (*15*). We also wanted to determine whether STM imaging in air can provide a more detailed understanding of Pt–I bonding interactions than has been obtained from extensive investigations of this system with LEED (low-energy electron diffraction), AES (Auger electron spectroscopy), SEXAFS (surface-extended x-ray absorption fine structure), and electrochemical measurements.

A brief review of previous surface analytical studies on this same system is desirable. Dosing of Pt(111) with iodine in UHV leads to the formation of two possible unit cells (*16, 17*), $(\sqrt{3} \times \sqrt{3})$, θ_I = 0.33 (structure **1**), and $(\sqrt{7} \times \sqrt{7})$, θ_I = 0.43 (structure **2**). Adsorption of iodine from a $10^{-3}M$ KI solution leads to the formation of (3 × 3), θ_I = 0.44 unit cell (structure **3**) (*18*). Indirect evidence from electrochemical characterization indicates that it is possible to form both structures **2** and **3** by annealing the surface in a H_2 flame and cooling it in a I_2-N_2 carrier gas stream (*19*). This latter procedure was developed as a means of preparing well-defined platinum surfaces for further electrochemical studies. Silver underpotential deposition (UPD) on surfaces prepared by this methodology displays the same current versus potential behavior as surfaces prepared in UHV (*20*). The silver UPD results suggest that the iodine dosing procedure can be used as replacement for the UHV ion bombardment and annealing procedure. All of the STM images we present were obtained on surfaces prepared through this non-UHV methodology (*21*).

The Pt(111) surface was cleaned and ordered in an atmosphere containing iodine (*19, 20*) in an apparatus equivalent to that described by Zurawski *et al.* (*19*). The iodine-dosed surfaces were electrochemically characterized with a Bioanalytical Systems CV-27 and reproduced published cyclic voltammograms of iodine-dosed Pt(111) surfaces (*16, 19*). The surface was imaged with a Nanoscope II (Digital Instruments, Santa Barbara, California) (*22*). The crystal was always oriented on the STM such that the rows of Pt atoms would be at angles of −30°, 30°, and 90° relative to the *x*-axis of the microscope scanner. A consistent and defined orientation of the crystal on the microscope stage greatly aided in image interpretation.

As received from Johnson Matthey, the polished face of the Pt(111) crystal was quite rough (60-nm vertical corrugation in a 200-nm scan range). No terrace structure was observable in the STM images. This result was not surprising, as a newly polished single crystal generally requires several days of ion bombardment and annealing in

Department of Chemistry, Purdue University, West Lafayette, IN 47907.

*To whom correspondence should be addressed.

UHV to obtain a well-ordered surface characterized by a sharp LEED pattern.

After cleaning in $HClO_4$, annealing in a H_2 flame, and cooling in an I_2-N_2 carrier gas stream, a regular terrace structure was observed on the Pt(111) surface that improved upon repeated applications of the procedure. The average terrace width was ~40 nm. On some regions of the crystal terraces up to 600 nm wide were imaged. The terrace length observed varied from 200 nm up to our 600-nm limited field of view. Measurements from several terrace images revealed a wide variation in step height, from single atom steps up to ten-atom steps. Other methods of surface preparation yielded very different terrace structures, generally with smaller terraces in the range of 6 to 20 nm.

We found it quite easy to obtain atomic resolution images of the iodine adlattices atop the Pt(111) surface using freshly etched tungsten tunneling probes. The atomic structure on top of narrow terraces (<15 nm) was difficult to image and was observed only fleetingly because of the nonideal structure of the tunneling probe tip. Imaging was more stable on top of wide terraces. The atomic structure on top of 40-nm or larger terraces was easy to image, with the majority of tungsten tunneling probe tips yielding high-resolution images.

In Fig. 1, A and B, two 3.6-nm topview images of the iodine-dosed surface are shown. No signal processing has been applied to either of these images. The images are uncorrected for thermal drift. Both images clearly show a repeating rhombic unit cell. The unit cell parameters measured from the images ($a = 0.715 \pm 0.03$ nm, $\alpha = 60° \pm 5°$, and $\theta = 16°$) are close to those expected for a $(\sqrt{7} \times \sqrt{7})$ unit cell ($a = 0.735$ nm, $\alpha = 60°$, and $\theta = 19.1°$). Examination of several images taken a few seconds apart indicated that the discrepancy in the unit cell parameters was caused by thermal drift. Large defect-free regions of the $\sqrt{7}$ structure (at least 50 nm by 50 nm) were observed on the surface. Interestingly, during the 4 months we spent imaging the iodine-dosed Pt(111) surfaces, we never observed a boundary between the two possible domains of the $(\sqrt{7} \times \sqrt{7})R19.1°$ unit cell. Although both domains were observed, they were always on different terraces.

The measured vertical corrugations observed for the $(\sqrt{7} \times \sqrt{7})$ unit cell varied considerably with the bias voltage and set point current used to acquire these images in the constant height mode (*21*). Calibrated vertical corrugations could be obtained from images acquired in the constant current mode (*2*); however, we have not yet obtained high-resolution, low noise images of this unit cell with that mode of microscope operation.

The differences between Fig. 1, A and B, illustrate the importance of exploring the operational parameter space of the STM. The image in Fig. 1B, taken at a set point current of 20.1 nA, shows three peaks corresponding to the three iodine atoms expected in the $(\sqrt{7} \times \sqrt{7})$ unit cell at coordinates (0,0), (1/3, 1/3), and (2/3, 2/3). However, images acquired at lower set point currents or higher bias voltages do not show all of the atoms in the unit cell, the image in Fig. 1A being one such example in which only the atom at coordinate (0,0) is clearly seen, with only a hint of an atom at (1/3, 1/3) and no evidence for the atom at (2/3, 2/3).

In Fig. 1C a height-shaded, three-dimensional surface plot of the data in Fig. 1B is presented after it has been digitally filtered to remove spacial frequencies below 0.25 nm. The view point is 30° off the surface normal. This presentation of the data clearly reveals the apparent height differences between the three peaks in the unit cell, which suggests two possibilities for the registration of the iodine adlattice with the Pt(111) substrate:

1) If we assume that the apparent height differences in the image reflect true topographic features of the structure, then one must register the hexagonal iodine lattice with the Pt substrate such that all of the iodine atoms occupy asymmetric sites.

2) If we assume that the apparent height differences are partially caused by differences in tunneling probability resulting from iodine-substrate bonding effects, then a structure in which all of the iodine atoms fall at high symmetry sites is possible.

Considering the second possiblity further: If the iodine atom at (0,0) is located atop a Pt atom, then the other two iodine atoms in the unit cell would be located at threefold hollow sites. The structure of the iodine adlattice would then conform to that proposed by Felter (*16*). In this structure, only one of the threefold sites occupied by an iodine atom is located above a second-layer Pt atom. The apparent height difference between the two iodine atoms in threefold sites can then be explained as an electronic effect due to the second layer of Pt atoms below the surface. Thus the tunneling probability above an iodine atom could be lowered by donation of electron density to the substrate when located directly above a second-layer Pt atom. Additional tunneling spectroscopic experiments and theoretical calculations of the local electronic structure are required to confirm this interpretation of the $(\sqrt{7} \times \sqrt{7})R19.1°$ images.

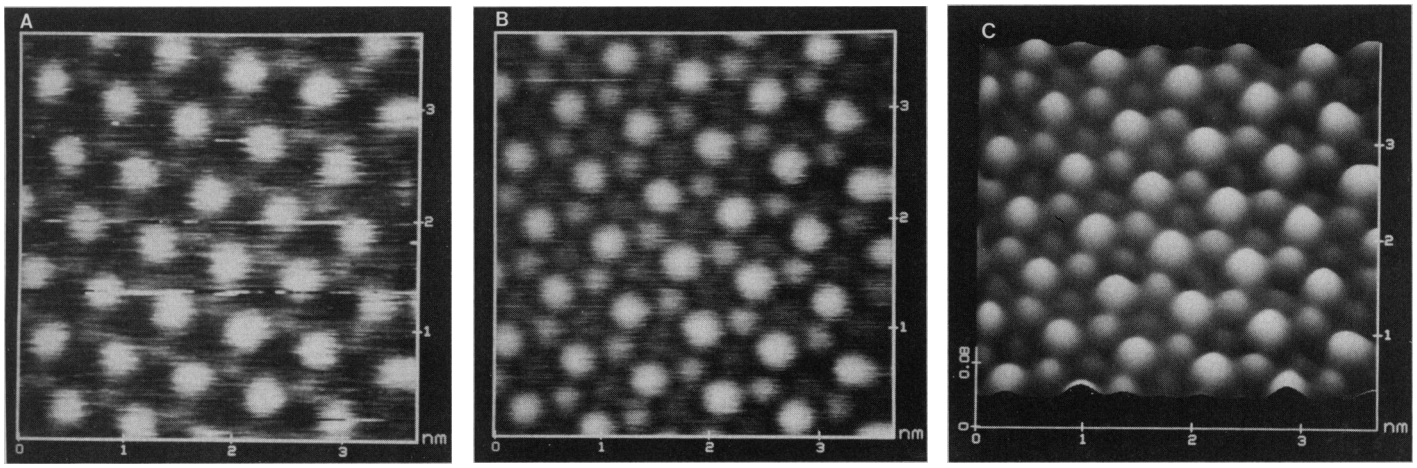

Fig. 1. Two 3.6-nm images of the Pt(111)–$(\sqrt{7} \times \sqrt{7})R19.1°$–I adlattice. Image (**A**) was recorded with a tip bias $V_t = 2.7$ mV and a tunnel current $i_t = 5.4$ nA, whereas image (**B**) was recorded with $V_t = 2.1$ mV and $i_t = 20.7$ nA. (**C**) A three-dimensional, height-shaded surface plot of the same image data as in (B). The viewpoint is 30° off of the surface normal. The data have been filtered in order to remove spatial frequencies below 0.25 nm.

At an iodine coverage of 0.44, the iodine is expected to form a (3 × 3) unit cell (*18–20*). We found that, by cooling the annealed Pt crystal only 2 mm from the iodine crystals in the dosing cell, the surface was predominately covered by (3 × 3) unit cells of two types that we call (3 × 3)–**1** and (3 × 3)–**2**. In Fig. 2 we present images for both (3 × 3) structures. A 3.6-nm topview image of (3 × 3)–**1** that was digitally filtered to remove spacial frequencies below 0.25 nm is shown in Fig. 2A. The same data is presented in Fig. 2B in a height-shaded, three-dimensional surface plot. Prior to filtering, the data was comparable in quality to that presented in Fig. 1. The four peaks in the unit cell at coordinates (0,0), (1/2, 0), (0, 1/2), and (1/2, 1/2), and their relative height differences can be explained only by one iodine atom adsorbed at an atop site and three atoms at twofold sites on the Pt surface. Such a structure exactly corresponds to that proposed by Katakaru *et al.* based on the unit cell determined from LEED and the iodine coverage determined electrochemically (*18*).

As stated above, two different (3 × 3) unit cell structures were observed. A topview image and a height-shaded surface plot of the (3 × 3)–**2** structure are shown in Fig. 2, C and D. The iodine atoms in the structure that corresponds to Fig. 2C do not form a regular hexagonal lattice as in the (3 × 3)–**1** structure (Fig. 2, A and B). We have not precisely determined the registry of the (3 × 3)–**2** unit cell with the Pt substrate; however, examination of images that contain domain boundaries between (3 × 3)–**1** and (3 × 3)–**2** unit cells should allow the assignment of the registry of the (3 × 3)–**2** structure.

An interesting defect appears in the images of the (3 × 3)–**1** adlattice (Fig. 2, A and B). Initial analysis points to the defect being related to the structure of the (3 × 3)–**2** unit cell (Fig. 2, C and D). In the defect, iodine atoms normally bonded to twofold sites are shifted a few tenths of an angstrom. The driving force for the rearrangement appears to be bonding of a formally twofold site iodine atom to a threefold site with other iodine atoms shifting into asymmetric sites to accommodate this change.

The two (3 × 3) structures were found in approximately equal proportion over the surface. We did not sense any preference for the iodine adlattice to form either of the two observed structures, nor could we find a variation of the dosing procedure that created predominately one of the two structures.

The observation of two (3 × 3) unit cell structures was unexpected on the basis of previous LEED and electrochemistry studies of this system. This study is a graphic illustration of the value of real space imaging provided by the STM. Although a complete discussion of the structure that best fits the image of the asymmetric (3 × 3)–**2** unit cell cannot be presented in this report, it is clear that I-I interatomic repulsions compete with I-Pt bonding forces to determine the adlattice structure. This study provides a striking example of the resolution that can be obtained with an STM operating in air. The STM can provide a suitable supplement to the standard UHV techniques, in this case providing much richer structural information. The images we report are currently being used as a benchmark against which the resolution that can be obtained during the in situ imaging of Pt electrode surfaces can be measured.

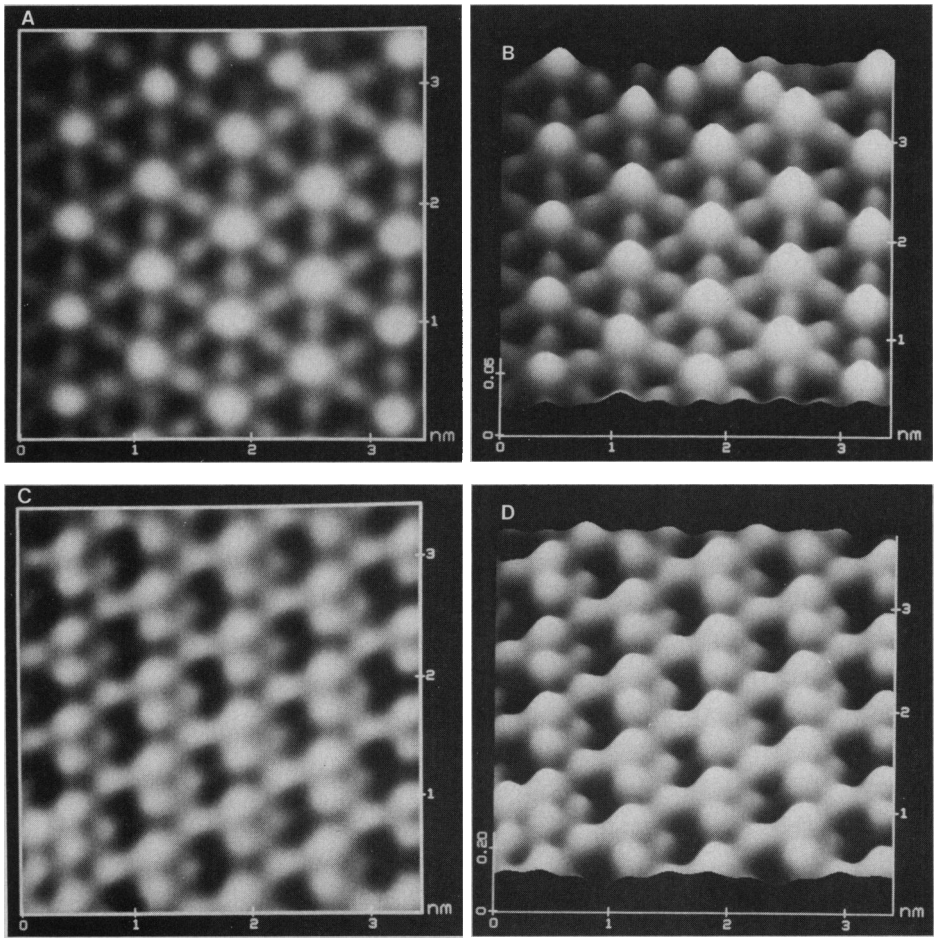

Fig. 2. Images of the Pt(111)–(3 × 3)–I adlattice. Image (**A**) was recorded with V_t =2.1 mV and i_t = 20.7 nA. The data has been filtered in order to remove spatial frequencies below 0.25 nm. Image (**B**) is a three-dimensional, height-shaded, surface plot of the same image data as in (A). The viewpoint is 30°C off of the surface normal. (**C**) Topview image of an alternate Pt(111)–(3 × 3)–I structure. The image was recorded with V_t = 5.8 mV and i_t = 17.1 nA. The image data have been filtered in order to remove spatial frequencies below 0.25 nm. (**D**) A height-shaded surface plot of the data in (C).

REFERENCES AND NOTES

1. G. Binnig, H. Rohrer, Ch. Gerber, E. Weibel, *Phys. Rev. Lett.* **49**, 57 (1982).
2. P. K. Hansma and J. Tersoff, *J. Appl. Phys.* **61**, R1 (1987).
3. H. Ohtani, C.-T. Kao, M. A. Van Hove, G. A. Somorjai, *Prog. Surf. Sci.* **23**, 155 (1986).
4. Y. Kuk and P. Silverman, *Appl. Phys. Lett.* **48**, 1597 (1986).
5. T. Sakurai *et al.*, *J. Vac. Sci. Technol. A* **6**, 803 (1986).
6. A. M. Baro *et al.*, *Phys. Rev. Lett.* **52**, 1304 (1984); G. Binnig, H. Fuchs, E. Stoll, *Surf. Sci.* **169**, L295 (1986); J. K. Gimzewski, E. Stoll, R. R. Schlittler, *ibid.* **181**, 267 (1987).
7. H. Ohtani, R. J. Wilson, S. Chiang, C. M. Mate, *Phys. Rev. Lett.* **60**, 2398 (1988).
8. R. Sonnenfeld and P. K. Hansma, *Science* **232**, 211 (1986).
9. R. Sonnenfeld and B. C. Schardt, *Appl. Phys. Lett.* **49**, 1172 (1986).
10. A. Gewirth and A. J. Bard, *J. Phys. Chem.* **92**, 5563 (1988).
11. V. M. Hallmark, S. Chaing, J. F. Rabolt, J. D. Swalen, R. J. Wilson, *Phys. Rev. Lett.* **59**, 2879 (1987).
12. B. Marchon *et al.*, *ibid.* **60**, 1166 (1988).
13. J. Wiechers, T. Twomey, D. M. Kolb, R. J. Behm, *J. Electroanal. Chem.* **248**, 451 (1988).
14. K. Itaya, S. Sugawara, K. Higaki, *J. Phys. Chem.* **92** 6714 (1988).
15. A. T. Hubbard, *Chem. Rev.* **88**, 633 (1988).
16. T. E. Felter and A. T. Hubbard, *J. Electroanal. Chem.* **100**, 473 (1979).
17. For an introduction into the terminology used for the specification of two-dimensional surface unit

cells, see G. A. Somorjai, *Chemistry in Two Dimensions: Surfaces* (Cornell Univ. Press, Ithaca, NY, 1981).
18. J. Y. Katekaru, G. A. Garwood, Jr., J. Hershberger, A. T. Hubbard, *Surf. Sci.* **121**, 396 (1982).
19. D. Zurawski, L. Rice, M. Hourani, A. Wieckowski, *J. Electroanal. Chem.* **230**, 221 (1987).
20. A. Wieckowski, S. D. Rosasco, B. C. Schardt, J. L. Stickney, A. T. Hubbard, *Inorg. Chem.* **23**, 565 (1984).
21. The Pt(111) single crystal disk was obtained from Johnson Matthey. Laue back-reflection x-ray photography was used to determine that the crystal was properly oriented within 0.5°. The Laue results were used to scribe a mark on the side and back face of the crystal to indicate the Pt substrate unit cell orientation.
22. The maximum scan range of the microscope head in both the x and y axes was 600 nm. All of the images shown were obtained in the constant height, fast-scan mode of the STM [A. Bryant, D. P. E. Smith, C. F. Quate, *Appl. Phys. Lett.* **48**, 832 (1986)]. The x-axis raster frequency was 156 Hz, with 200 or 400 scan lines per image. The images reported have had a least-squares plane subtracted to remove any tilt of the microscope head relative to the sample surface. Images are presented as a gray scale proportional to the natural logarithm of the measured tunneling current; the measured current increases from black to white. The tunneling probe tips were made from tungsten wire, 0.025 cm in diameter, etched in 1*M* KOH at 10 V and 60 Hz ac.
23. Supported by the Industrial Associates program at Purdue University funded in part by Dow Chemical Co. and BP America, and a Basic Research Grant from Chevron Research Company.

6 December 1988; accepted 28 December 1988

Uranium-Series Dated Authigenic Carbonates and Acheulian Sites in Southern Egypt

B. J. SZABO, W. P. MCHUGH, G. G. SCHABER, C. V. HAYNES, JR., C. S. BREED

Field investigations in southern Egypt have yielded Acheulian artifacts in situ in authigenic carbonate deposits ($CaCO_3$-cemented alluvium) along the edges of now-aggraded paleovalleys (Wadi Arid and Wadi Safsaf). Uranium-series dating of 25 carbonate samples from various localities as far apart as 70 kilometers indicates that widespread carbonate deposition occurred about 45, 141 and 212 ka (thousand years ago). Most of the carbonate appears to have been precipitated from groundwater, which suggests that these three episodes of deposition may be related to late Pleistocene humid climates that facilitated human settlement in this now hyperarid region. Carbonate cements from sediments containing Acheulian artifacts provide a minimum age of 212 ka for early occupation of the paleovalleys.

THE AREA WEST OF THE NILE (FIG. 1) is barren of human occupation and is one of the most arid regions on earth. However, aggraded paleovalleys, parts of ancient drainage systems, have been identified recently through the use of space shuttle imaging radar (SIR) (*1, 2*). During subsequent field expeditions to investigate the radar geology of these paleovalleys (*2–4*), we discovered many Acheulian (lower Paleolithic) sites both on the surface and buried in alluvium along the edges of several of these features. The sedimentary contexts of the buried Acheulian sites indicate that the groundwater table was shallow during periods of Acheulian occupation. Extensive carbonate (calcrete) was deposited by this ground water, ultimately cementing the alluvial sand and gravel and some of the artifacts. In this report, we present uranium-series (U-series) dates of this authigenic carbonate that provide a preliminary basis for dating episodes of carbonate deposition, pluvial climatic phases, and artifacts incorporated in the sediments relating to the settlement of the area by early man.

Archeological sites, especially Holocene-age Neolithic sites, are abundant along the edges of the ancient valleys and in the intervening interfluves (*5*); they provide evidence of a long but discontinuous occupation of this region. Geoarchaeological evidence indicates that there were several episodes of climatic and cultural change in the region since the last stages of valley aggradation more than 0.2 million years ago (*6*).

We have studied two of the radar valleys (wadis) in the heart of the hyperarid Eastern Sahara (Fig. 1): Wadi Arid ("wide wadi," about 15 km wide, 100 km long, and 350 km west of Lake Nasser) and Wadi Safsaf (including Bir Safsar, about 70 km northeast of Wadi Arid). Seismic data indicate that Wadi Arid is filled by several hundred meters of sediment above bedrock (*7*). A series of braided channels, possibly Holocene, is inset into the large Safsaf valley (*3*). A bedrock divide covered by sand sheet deposits is thought to separate Wadi Safsaf from Wadi Arid (*2, 6*). The upper parts of the valley fill of both Wadi Arid and Wadi Safsaf consist of sand and small gravel alluvium below a thin sand cover that is transparent to the SIR sensor (*1, 3*).

In 10 of 36 backhoe trenches (BHTs) along the southeast edge of Wadi Arid (Fig. 2) we found artifacts at depths of 1 to 3 m; three BHTs yielded hand axes, the diagnostic Acheulian artifact. Only one BHT in the middle of the wadi yielded artifacts. Along the northwest margin of the wadi, the upper part of the valley fill has been eroded away exposing a strongly carbonate-cemented terrace (Fig. 2) on which several Acheulian sites were found. Test pits dug in this terrace (site 84F21-7) yielded handaxes and other artifacts at shallow depths (to 50 cm), including four large middle Acheulian hand axes from a loose, noncemented sheetwash deposit (*8*).

Backhoe excavations in Wadi Safsaf allowed the determination of the features in the filled inset channels and the valley fill (*3*) that were responsible for the SIR images, but they yielded no artifacts from strata that could be dated accurately. In addition to the many Neolithic sites among the braided channels, we found few middle Paleolithic sites in the area and some extensive Acheulian sites around the perimeter of Bir Safsaf (*6, 8*) and in a depression south of Wadi Safsaf. Brief investigation of one of these sites southeast of Bir Safsaf yielded two late Acheulian (*6, 8*) hand axes in situ in a loose, carbonate-impregnated sandy matrix.

The bedrock bordering Wadi Arid and Wadi Safsaf is mostly quartzitic sandstone that contains no calcium carbonate (*9*). The source of the calcium in the secondary calcite may be airborne dust that was transported from the Eocene limestone plateau northeast of the radar valleys (Fig. 1). The processes involved in the carbonate cementation of the valley fill are not yet clear. McCauley *et al.* (*2*) and Haynes (*10*) have concluded that most secondary carbonate deposits (calcretes, nodules, and carbonate cements in

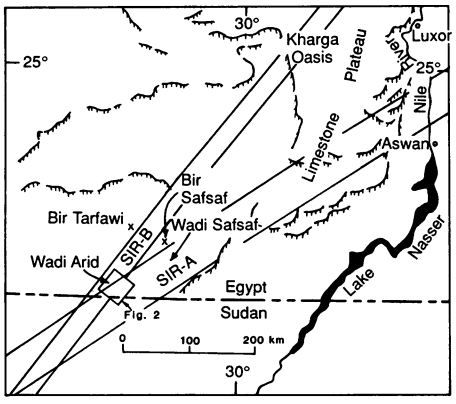

Fig. 1. Map showing location of paleovalley study areas and SIR groundtracks in southern Egypt.

B. J. Szabo, U.S. Geological Survey, Box 25046, Mail Stop 963, Denver, CO 80225.
W. P. McHugh, EPIX Incorporated; 571 Coal Street, Wilkinsburg, PA 15221.
G. G. Schaber and C. S. Breed, U.S. Geological Survey, 2255 North Gemini Drive, Flagstaff, AZ 86001.
C. V. Haynes, Department of Anthropology, University of Arizona, Tucson, AZ 85721.